

Revealing the Mechanical Impact of Biomimetic Nanostructures on Bacterial Behavior

Xin Wu¹, Xianrui Zou¹, Donghui Wang², Mingjun Li², Bo Zhao¹, Yi Xia^{2,*}, Hongshui Wang^{2,*} and Chunyong Liang^{1,*}

¹ Tianjin Key Laboratory of Materials Laminating Fabrication and Interface Control Technology, School of Materials Science and Engineering, Hebei University of Technology, Tianjin 300130, China.

xinwu1209@163.com (X.W.); zouxianrui@163.com (X.Z.); z15079039978@163.com (B.Z.)

² Center for Health Science and Engineering, Hebei Key Laboratory of Biomaterials and Smart Theranostics, School of Health Sciences and Biomedical Engineering, Hebei University of Technology, Tianjin 300131, China; donghuiwang@hebut.edu.cn (D.W.); mjli@hebut.edu.cn (M.L.)

* Correspondence: xiayi@hebut.edu.cn (Y.X.); kingflood@hebut.edu.cn (H.W.); liangchunyong@hebut.edu.cn (C.L.)

* Correspondence: Email: xiayi@hebut.edu.cn(Y.X.) Email: kingflood@hebut.edu.cn (H.W.)Email: liangchun-yong@hebut.edu.cn(C.L.)

Supporting Table and Figures

Figure S1. Cicada surface structure characterization.

Figure S2. AAO template SEM images.

Figure S3. SEM images of four surfaces at different magnifications.

Figure S4. 2D cross-section images in AFM of different surfaces.

Figure S5. Cu²⁺ release amounts after soaking different structured surfaces in PBS for 1 day.

Figure S6. Surface area size at 5 × 5 μm detection range for different surfaces.

Figure S7. Shape and size parameters of geometric models. (a) *E. coli*; (b) *S. aureus*.

Figure S8. Schematic diagram of the process of 3D reconstruction of nanostructured surfaces.

Figure S9. Setting of boundary conditions for the finite element model.

Figure S10. Locally refined mesh models of the contact areas: (a) *E. coli*; (b) *S. aureus*.

Table S1. Intrinsic modeling of materials in finite element models.

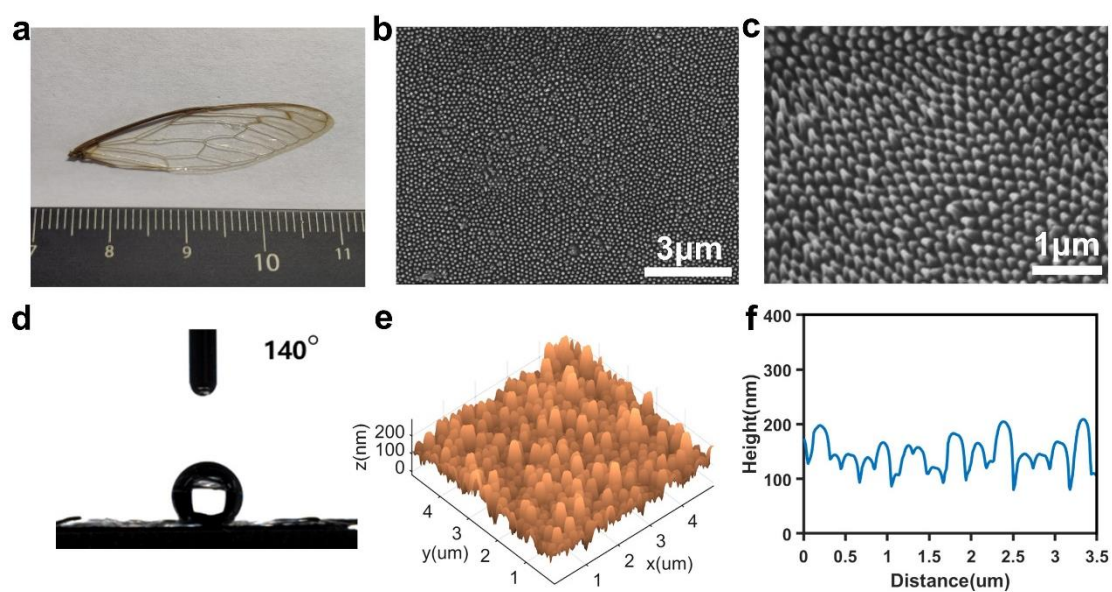


Figure S1. Cicada surface structure characterization. (a) Physical image of a cicada wing. (b-c) SEM images of the surface structure of the cicada wing at different magnifications. (d) Static water contact angle on the surface of the cicada wing. (e-f) AFM images of cicada wing surface.

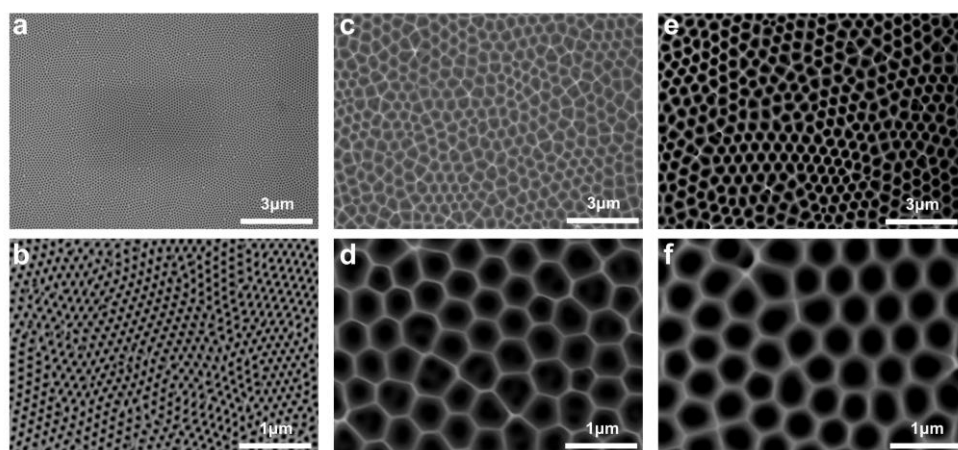


Figure S2. AAO template SEM images. (a-b) NP1; (c-d) NP2; (e-f) NP3.

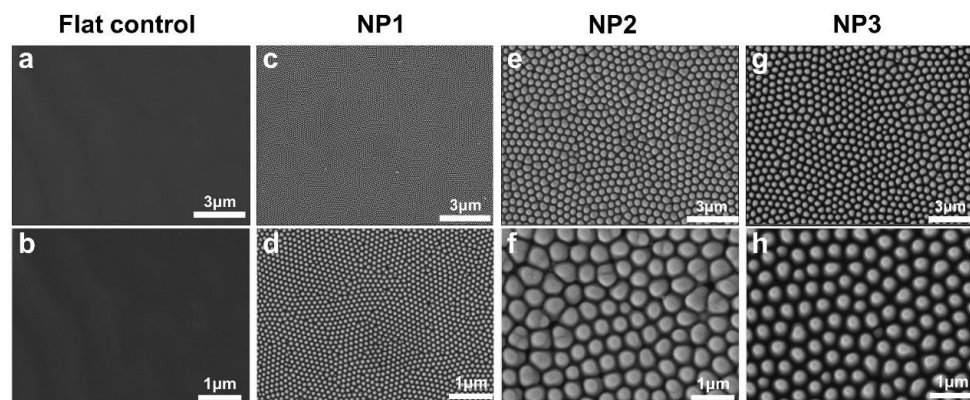


Figure S3. SEM images of four surfaces at different magnifications. (a-b) flat; (c-d) NP1; (e-f) NP2; (g-h) NP3.

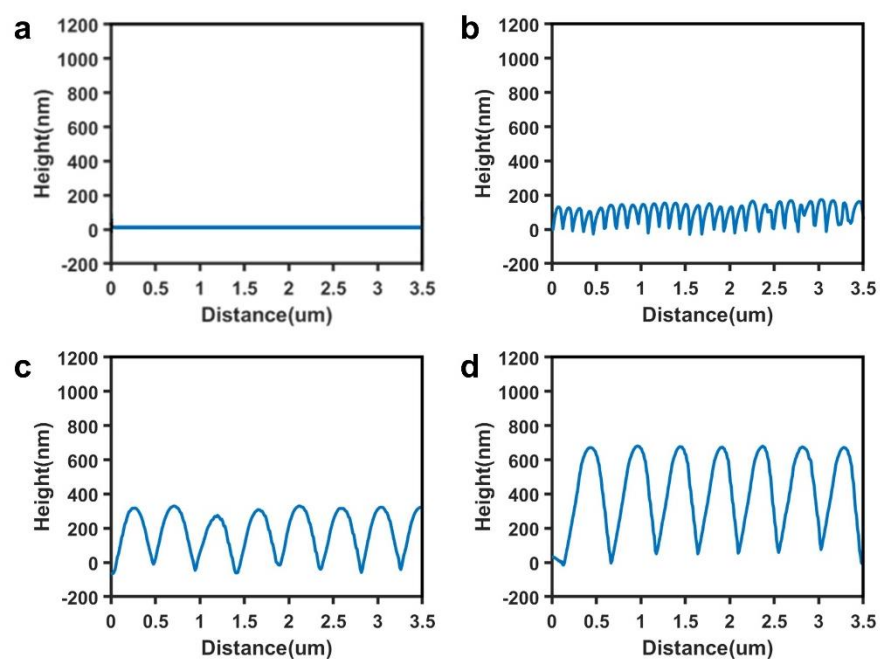


Figure S4. 2D cross-section images in AFM of different surfaces. (a) flat; (b) NP1; (c) NP2; (d) NP3.

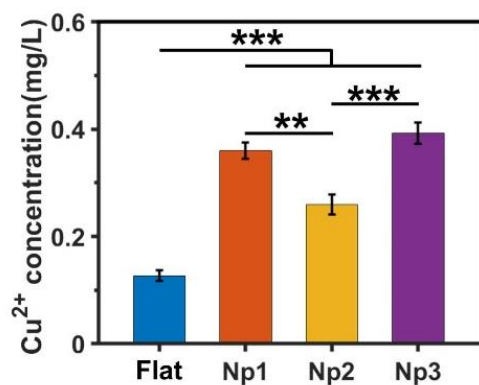


Figure S5. Cu^{2+} release amounts after soaking different structured surfaces in PBS for 1 day.

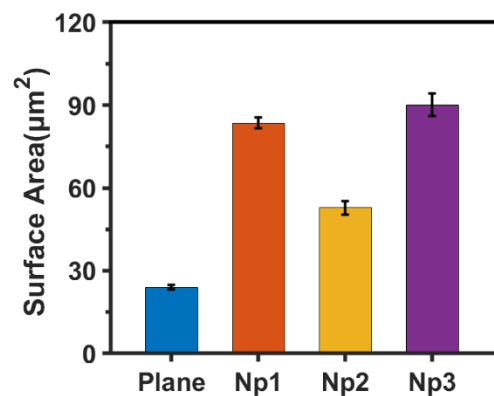


Figure S6. Surface area size at $5 \times 5 \mu\text{m}$ detection range for different surfaces.

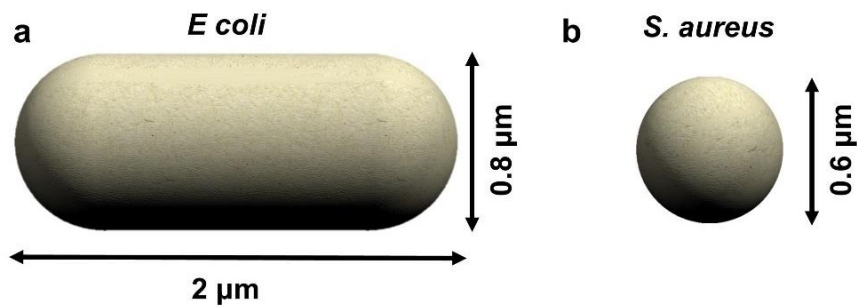


Figure S7. Shape and size parameters of geometric models. (a) *E. coli*; (b) *S. aureus*.

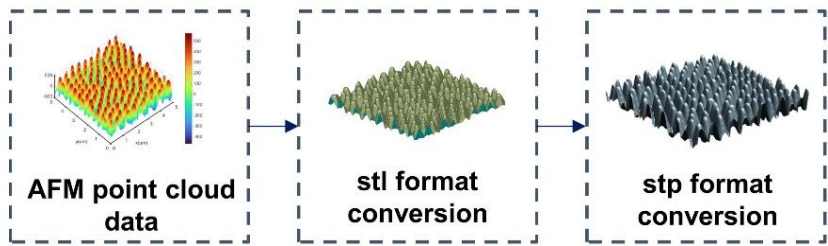


Figure S8. Schematic diagram of the process of 3D reconstruction of nanostructured surfaces.

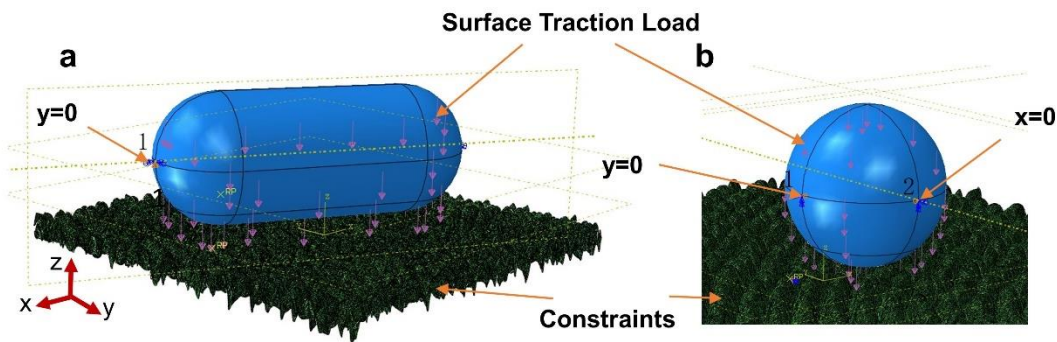


Figure S9. Setting of boundary conditions for the finite element model.

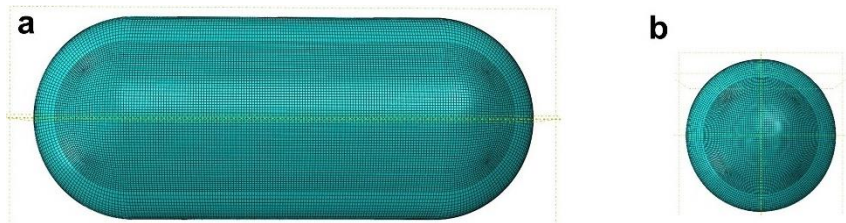


Figure S10. Locally refined mesh models of the contact areas: (a) *E. coli*; (b) *S. aureus*.

Table S1. Intrinsic modeling of materials in finite element models.

Part	Material Model	Parameter	Element type	Reference
Cell wall	Orthotropic Elastic	$E_1=30\text{ MPa}$; $E_2=E_3=15\text{ MPa}$; $\nu_{12}=\nu_{13}=\nu_{23}=0.35$; $G_{12}=G_{13}=5.3\text{ MPa}$; $G_{23}=3.7\text{ MPa}$	C3D8RH	[1]

Cytoplasm	Hyperelastic (Neo-Hookean)	$C_{10}=0.71$ MPa	C3D8RH	[2]
Nanostructured surfaces	Discrete rigid	-	R3D3	-

References

1. Velic A, Hasan J, Li Z, et al. Mechanics of bacterial interaction and death on nanopatterned surfaces [J]. Biophysical Journal, 2021, 120(2): 217-31.
2. Bavi N, Nakayama Y, Bavi O, et al. Biophysical implications of lipid bilayer rheometry for mechanosensitive channels [J]. Proceedings of the National Academy of Sciences, 2014, 111(38): 13864-9.